

Study of Ionospheric Variability during Super Substorms

D. Pandit, N. P. Chapagain and B. Adhikari

Journal of Nepal Physical Society

Volume 6, Issue 2, December 2020

ISSN: 2392-473X (Print), 2738-9537 (Online)

Editors:

Dr. Binod Adhikari

Dr. Bhawani Joshi

Dr. Manoj Kumar Yadav

Dr. Krishna Rai

Dr. Rajendra Prasad Adhikari

Mr. Kiran Pudasainee

JNPS, **6** (2), 74-84 (2020)

DOI: <http://doi.org/10.3126/jnphysoc.v6i2.34862>

Published by:

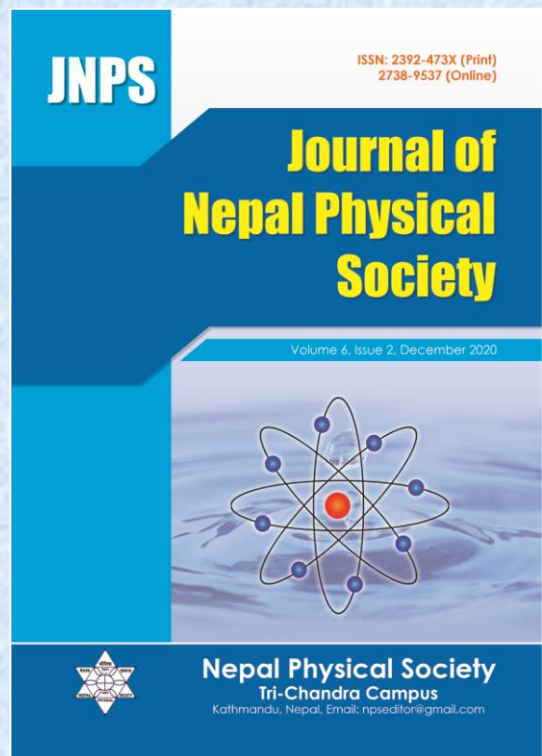
Nepal Physical Society

P.O. Box: 2934

Tri-Chandra Campus

Kathmandu, Nepal

Email: npseditor@gmail.com





Study of Ionospheric Variability during Super Substorms

D. Pandit^{1,3}, N. P. Chapagain² and B. Adhikari³

¹Central Department of Physics, IOST, Tribhuvan University, Kirtipur, Kathmandu, Nepal

²Amrit Campus, Thamel, Kathmandu, Nepal

³St. Xavier's College, Maitighar, Kathmandu, Nepal

Corresponding Email: drabindra@sx.edu.np

Received: 12 October, 2020; Revised: 15 November, 2020; Accepted: 25 December, 2020

Abstract

This paper study variability of three ionospheric parameters foF2, h'F and hmF2 to investigate the middle latitude ionospheric effect at Boulder, Colorado, USA (40°N, 1105.0° W) during super substorms (SSSs) of 24 August 2005, and 7 September 2017 and 8 September 2017 respectively. Continuous wavelet transform (cwt) implemented to identify the low and high frequency and longer and shorter duration present in the signal. The result shows decrease in foF2 during SSSs of 24 August 2005 and 8 September 2017 and increase in foF2 during 7 September 2017. The highest fluctuation in h'F is noticed during SSS of 24 August 2005. The cwt shows that the coupling between solar wind and magnetosphere occurs between ~ 16 to 32 minutes for SSS of 24 August 2005 and between 27.9 to 64 minutes during super substorm of 7 and 8 September 2017 for all the ionospheric parameters respectively. This study leads to understand the impact of SSSs on communication signals due to energy injected in ionosphere during the coupling mechanism between magnetosphere-ionosphere.

Keywords: Magnetosphere, Ionosphere, continuous wavelet transform, Super sub-storm.

1. INTRODUCTION

Ionosphere is highly vulnerable region affected by a) solar ionizing radiation (solar rotation variation, solar cycle variation and formation and decay of active region); b) neutral atmosphere (acoustic and gravity wave, planetary waves, surface phenomena like earthquakes and volcanic eruption); c) electrodynamics (dynamo effects of low latitude phenomena, penetration of magnetospheric electric field, electric field from lightning and sprites); d) solar wind geomagnetic (magnetic storm, substorms, IMF/solar wind sector structure, energetic particle precipitation and Joule heating). The present study emphasizes on ionospheric variability during very intense substorm called Super Substorm (SML < -2500 nT) [1], it is crucial for the researchers to understand the physical interaction processes in solar wind-Earth's magnetosphere-ionosphere system during this event. The huge injected energy accompanied with super substorm will result in thermospheric and ionospheric storms. The ionosphere during this super substorm will change in

complex ways resulting change in its critical frequency (foF2), maximum electron density height (hmF2) and virtual height (h'F). Many past researchers reported that the storm-time ionosphere changes in rather complicated ways. Due to its complexity its underlying physical processes are far from being fully understood. In 1997, Lakshmi [2] studied the response of the great storm of 13 March 1989 using ionosonde data over the equatorial and F-region in India. In 2002, Pincheira [3] studied the responses of magnetic storm on ionosphere and thermosphere over the South American sector using foF2, hmF2 and neutral winds extracted from measured hmF2, using interhemispheric plasma model. In Brazilian sector de Abreu et al, 2014a, b, c found that the occurrence of ESFs are closely related to daily variations of the h'F near equator. The relationship between spread-Fs and other ionospheric parameters, foF2 and h'F variations with the spread-Fs have been studied by Rungraengwajjake [7], Smith [8], Liu and Shen [9]. The seasonal, solar and magnetic activity variabilities on h'F threshold have been investigated by Manju [10] and Narayanan [11,

12]. In 2020, Li studied the contribution of geomagnetic activity to ionospheric foF2 at different phases of solar cycle by spectral whitening method.

Many studies on storm, substorm has conducted for ionospheric parameters in different latitudes however no result for the SSSs on ionospheric parameters have been reported up to now. The list of researchers carried research on other area of SSSs are Tsurutani [1]; Hajra [13]; Adhikari [14-16]; Despirak [17, 18]; Tsurutani [19]. In this paper, we report for the first time the ionospheric responses during the 24 August 2005 and 7 and 8 September 2017 super substorm using ionosonde data measured at Boulder, Colorado, USA (40.0° N, 105.0° W). A brief description of data selection for these events is described in section 2. The results and discussion are presented in the section 3 and the conclusions of this work are summarized in section 4.

2. A BRIEF DESCRIPTION OF THE DATASET AND METHODOLOGY

2.1 Datasets

The three SSSs occurred on 24 August 2005, 7 September 2017 and 8 September 2017 were analyzed for the present study. Their corresponding interplanetary, solar wind and geomagnetic data is downloaded from <http://nssdc.gsfc.nasa.gov/omniweb> database. To study the impact of SSSs on mid latitude the F-region parameters: critical frequency (foF2), virtual height (h'F) and height of peak electron density over Boulder, Colorado, USA (40.0° N, 105.0° W) is analyzed in relation to quiet-day values of these parameters closest to the respective storm times. The table 1 gives the list of the days including a reference quiet day for three SSSs. The ionosonde data for these parameters were downloaded from Global Ionospheric Radio

Observatory (GIRO) website <https://ulcar.uml.edu/DIDBase/>.

2.2 Methodology

The continuous wavelet transform technique (cwt) is used to identify the singularity and transient structure present in the time series data. The signal energy in wavelet space is represented in scalogram using a log2 function. It allows the decomposition of data, functions or operators into different frequency or scale component [20] and each component present can be studied with its resolution which matches with its scale. The high and low frequency wavelet is very narrow and broad. Hence, it is a good technique to zoom in the short lived high frequency present as singularities and transient structures. The frequencies associated with wavelet transform detect the respective frequencies of the super substorms. The amplitudes of the wavelet coefficients are small [21] for smooth signals but for the singularities and transient structures it has larger amplitude. In the signal processing scalogram is used to visualize the square of the amplitude of the coefficient which illustrates as the distribution of signal energy in time t and scale a [14-16]. In this work, we identify quiescent and non-quiescent periods related to SSSs.

If a and b represent the dilation and translation parameters that vary continuously, then the continuous wavelet transform becomes

$$W(a, b) = \int f(t) \varphi * \left(\frac{t-b}{a} \right) dt \quad (1)$$

where $\varphi *$ represents complex conjugate of φ and the function $W(a, b)$ represents the wavelets coefficients. For $a > 0$, variation of scale parameter gives dilation effect and for $a < 0$, it gives contraction effect of the mother wavelet function. Hence, it is convenient to identify the low and high frequency and longer and shorter duration present in the signal.

Table 1: Geographic and Geomagnetic Coordinates of ionosonde station.

Station	Geographic Latitude	Geographic Longitude	Geomagnetic Latitude	Geomagnetic longitude
Boulder	40.00° N	105.00° W	47.54° N	37.47° W

Table 2 : The list of study days including reference quiet days for each of the three storms.

Event	SSS day	Reference quiet day
1	24 August 2005	20 August 2005
2	7 September 2017	28 September 2017
3	8 September 2017	28 September 2017

3. RESULT AND DISCUSSION

In this section, we discuss and present the interplanetary, solar wind and geomagnetic data and the disturbance variations on the parameters foF2, h'Fand hmF2 during each SSS.

3.1 SSS of 24 August 2005

Figure 1 shows the time profile of solar wind parameters and geomagnetic indices of SSS 24 August 2005. The top three panels represent the variation of Vsw, T and Psw/Nsw (combined in panel three) while the bottom five panels show the variation in B/Bz, Ey, AE, SYM-H and AU/AL respectively. The sharp decrease in AL at 10:20 UT indicates the position of SSS. At the

peaks the value of AL is -3954 nT. The value of SYM-H at the onset time of first SSS is +95 nT where its value goes to -170 nT during its peak value of AL. During the onset of the IMF Bz has turned towards southward direction. The value of Vsw, Tsw, Nsw, Ey and AE during the onset of event was ~ 600 Km/s, ~ 5×10^5 K, ~ 5 cm^{-3} , ~ 35 mV/m and ~ 3800nT respectively. It is seen from the plot that magnetosphere is much more sensitive to the solar wind dynamic pressure variations when the IMF is strongly southward than when it is weakly southward which trigger the release of the stored energy during southward field [1].

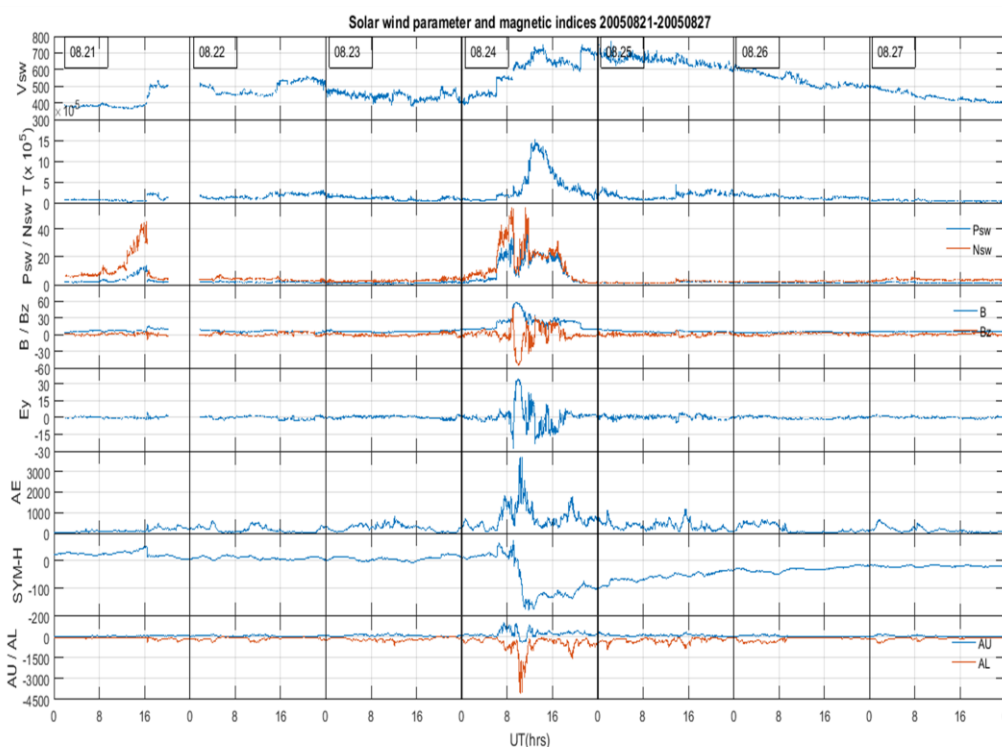


Fig. 1. From top to bottom shows the variations of solar wind speed (Vx in Km/s), temperature (T in K), pressure (Psw in nPa), plasma density (Nsw in cm^{-3}), total magnetic field (B, nT) interplanetary magnetic field IMF (Bz in nT), interplanetary electric field (Ey in mV/m), auroral index (AE in nT), SYM-H (in nT), aurora up (AU in nT) and aurora low (AL in nT) characterizing super substorm 21-27 August 2005 respectively.

3.2 SSS of 7 and 8 September 2017

In early September 2017, it was found a rapid development of group of sunspots and solar flare of class X9.3 and eruption of series of coronal mass ejection (CME) from the Sun. The solar flares M9.3 (4 September), X2.2 and X9.3 (6 September), M7.3 and X1.3 (7 September), M8.1 (8 September) and X8.2 (10 September) were identified respectively. First CME was detected in the morning of September 7 and a second CME was identified in

afternoon of September 8. Figure 2 shows the time profile of solar wind parameters and geomagnetic indices on 7-8 September 2017. The top three panels represent the variation of solar wind velocity (Vsw in Km/s), temperature (T in K) and pressure (Psw in nPa)/ density (Nsw in m^{-3}) (combined in panel three) while the fifth panels show the variation in total magnetic field and interplanetary magnetic field B (in nT) /Bz (in nT), electric field (Ey in mV/m), AE , SYM-H and AU/AL in nT

respectively. The two sharp decrease in AL noticed on September 7 at ~23:45 UT and on 8 at ~13:00 UT with $AL < -2500$ nT indicate the position of two SSSs. The value of SYM-H at the onset time of first SSS is -145 nT during its peak value of AL and during second SSS the value of SYM-H noticed is -100nT. During the onset of September 7 SSS was intense because IMF Bz has turned intensively towards southward direction than on SSS of September 8. The value of Vsw, Tsw, Nsw, Ey and AE during the onset first and second event was ~ 575 Km/s, ~ 10^6 K, ~ 6 cm^{-3} , ~ 25 mV/m and ~ 2500nT ; ~ 750Km/s, ~ 5×10^5 K, ~ 7 cm^{-3} , ~

10mV/m and ~ 2700nT respectively. The two events are isolated and large [1], duration of the first and the second event is ~15 minutes and ~25 minutes respectively. The interplanetary sheath is the causative of SSS events of September 7 and magnetic cloud of the September 8 [17]. Multiple magnetic fluctuations are the signature of sheath region. Similar to the figure 1, the figure 2 shows that magnetosphere is much more sensitive to the solar wind dynamic pressure variations when the IMF is strongly southward than when it is weakly southward which trigger the release of the stored energy during southward field [1].

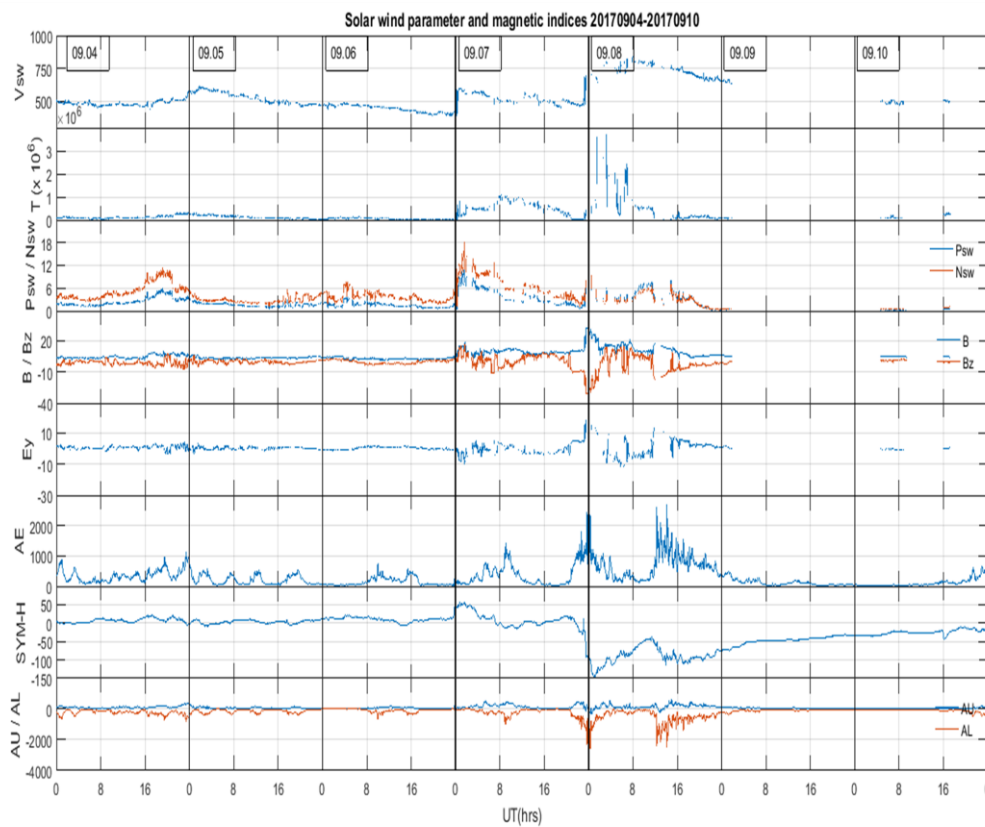


Fig. 2. From top to bottom shows the variations of solar wind speed (V_x in Km/s), temperature (T in K), pressure (Psw in nPa), plasma density (Nsw in cm^{-3}), total magnetic field (B, nT) interplanetary magnetic field IMF (Bz in nT), interplanetary electric field (Ey in mV/m), auroral index (AE in nT), SYM-H (in nT), aurora up (AU in nT) and aurora low (AL in nT) characterizing super substorm 4-10 September 2017 respectively.

3.3 Ionospheric responses

The ionospheric observations to the SSSs of 24 August 2005, 7 September 2017 and 8 September 2017 are shown in figure 3, 4 and 5 respectively. The dotted line in each figure represents the quiet day variation and the solid line represents ionospheric variability during SSSs. From the figure 3, it is observed the decrease in the foF2 but enhancement in h' F and hmF2 during SSS of 24 August 2005 in compared with the quiet day. The

observed value of foF2, h' F and hmF2 during SSS of 7 September 2017 is found higher than quiet day in figure 4. And in figure 5, the value of foF2 and hmF2 measured during SSS of 8 September 2017 higher than quiet day value but h' F is observed lower than the quiet day. In 2015, Tsurutani [1] assumed that energy stored in magnetosphere/magnetotail during southward turning of IMF Bz released by plasma parcel during

SSSs result strongest ionospheric current during this events, potentially causing power outage on the Earth. Long term data 1981-2012 on SSSs was

analyzed by Hajra [13] and found that SSSs can occurs in any phase of the solar cycle but it highest rate is 3.8 year^{-1} in the descending phase.

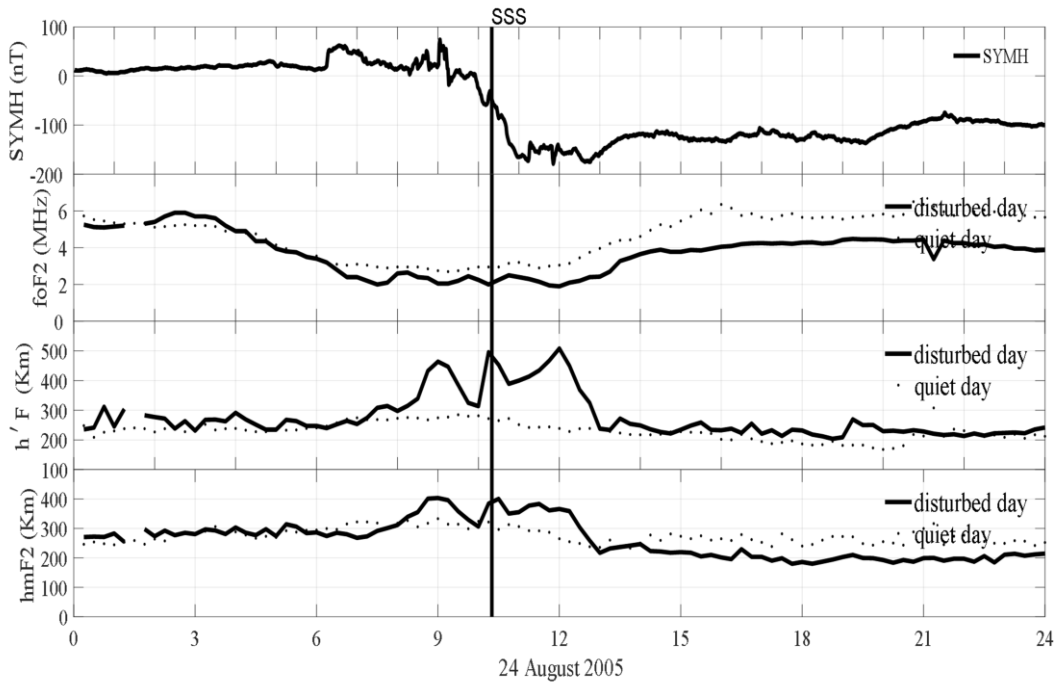


Fig. 3. Variation in SYMH (nT), critical frequency (foF2 in MHz), virtual height(h'F in Km) and height of peak electron density (hmF2 in Km). The dotted line represents the quiet day variation and the solid line represents the variations on the SSS day of 24 August 2005.

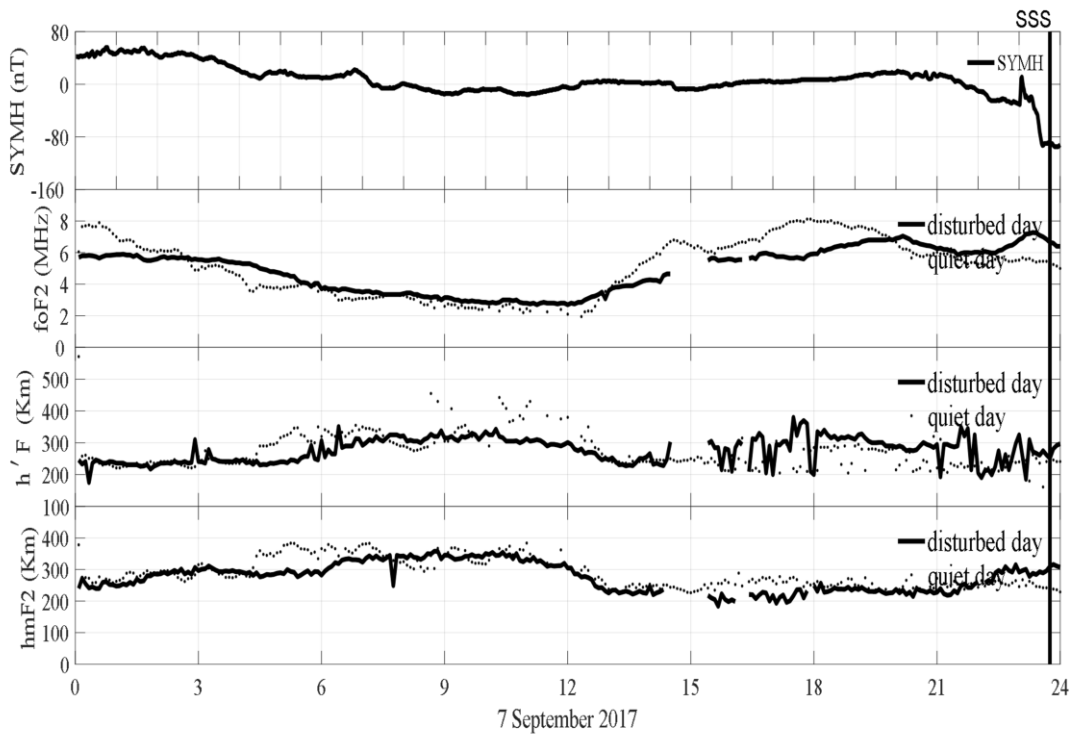


Fig. 4. Variation in SYMH (nT), critical frequency (foF2 in MHz), virtual height(h' F in Km) and height of peak electron density (hmF2 in Km). The dotted line represents the quiet day variation and the solid line represents the variations on the SSS day of 7 September 2017.

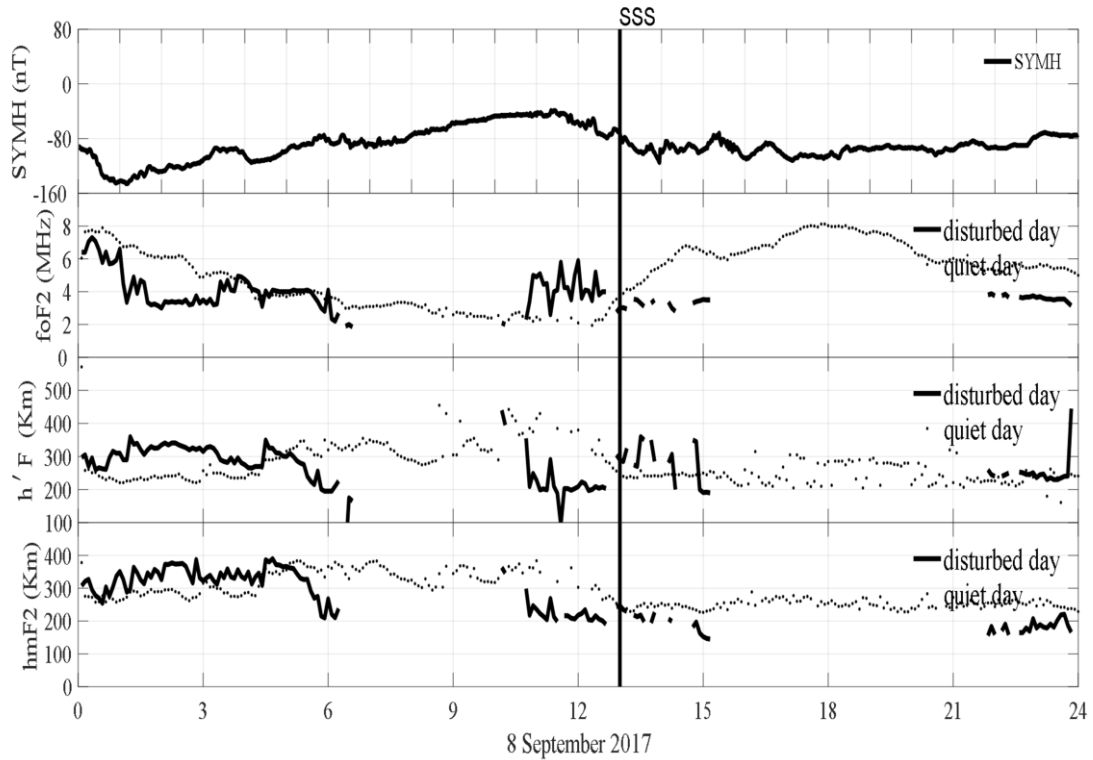


Fig. 5. Variation in SYMH (nT), critical frequency (foF2 in MHz), virtual height(h' F in Km) and height of peak electron density (hmF2 in Km). The dotted line represents the quiet day variation and the solid line represents the variations on the SSS day of 8 September 2017.

Their study shows the intensity of SSSs occurrence is independent to the intensity of magnetic storm and also found that the SSSs which occur during main phase of geomagnetic storm causes strong ionospheric current even at low latitude may cause of power outage on the Earth. A strong ionospheric current induces large fluctuation in $\frac{\partial B}{\partial t}$ in power transmission line induces GIC causes power outage during intense magnetic storm [1]. The study of polar cap potential and polar cap index during SSSs by Adhikari [15] found that polar cap potential and merging electric field are excitingly high and it is 20 time higher than the potential developed during HILDCAA. Their study further concluded that heavily increase in field aligned current during SSSs produces intense aurora which may disrupt and jammed the communication signals and large potential drop during these events may cause serious and rapid change in space weather condition. In total 131 SSSs event between 1998-2016 were studied by Despirak [18] and observed SSSs during interplanetary manifestation of coronal mass ejection ie sheeth (45.2%), magnetic cloud (42%) and ejecta (8.3%) none of the SSS event was identified during high speed streamer from coronal hole (CIR). The two SSSs

of 7 and 8 September 2017 was studied by Despirak [17] using SuperMAG electric field and found that the ionospheric current observed in global scale around the Earth during the event. In 2019, Poudel [22] studied the average energy deposited inside the magnetosphere during substorm (5.5199×10^{11} W), intense storm (5.3365×10^{11} W), HILDCAA (3.4618×10^{11} W), super substorm (1.0367×10^{12} W) and quiet day (5.8772×10^{10} W) found that the highest amount of energy deposited during super sub storm which may causes intense ionospheric storm to produced change in ionospheric parameters. The contribution of geomagnetic activity to ionospheric foF2 trends at different phases of the solar cycle was studied by Li [23] and found that the impact to the ionosphere is maximum during maximum geomagnetic activity, which usually happens in the declining phase of the solar cycle. The SSSs of 2005 and 2017 lay in the declining phase of the solar cycle 23 and 24.

The phenomena of positive and negative ionospheric storm causes increase and decrease in foF2 [24]. The positive and negative ionospheric storms effects are local time local time dependent [25, 26]. The change in neutral composition [27,

28] during geomagnetic storm influences negative ionospheric storm [29, 30, 31]. In 1993, Prolss [32] postulated that the positive ionospheric storm is caused by meridional wind negative ionospheric storm is caused by change in neutral composition. The energy deposited at polar latitude during geomagnetic storm produces a travelling ionospheric disturbance which superimpose with gravity waves and travel with high speed towards the equator causing day time positive ionospheric storm lifting daytime F2 layer to higher altitude. The energy deposited at polar latitude during solar wind may introduce compositional change which expands equator wards and produces F2 layer disturbance at middle latitude.

3.4 Continuous wavelet transform

Figure 6a, b and c represent scalogram for the critical frequency (foF2 in MHz), virtual height (h' F in Km) and height of peak electron density (hmF2 in Km) during SSSs of 24 August 2005, 7 September 2017 and 8 September 2017. In the figures, the horizontal axis represents the time in hour and the vertical axis represents the periodicity in minutes. The amplitude represented in the plot whose color are demonstrated on the right side have units in their square for F2 layer critical frequency (foF2), virtual height (h' F) peak density height (hmF2). The figure 6a show the power areas of the highest intensity more continuously at time scales approximately between 16-32 minutes during the SSS ~ 10:20 UT of 24 August 2005. In this region the background intensity is found to increased from 0.5 to 1.5 (nT)² foF2. Similarly, figures 6b and 6c the background intensity increased from 0.5 to 2 (nT)² in h' F and 0.5 to 1.5 (nT)² in hmF2 respectively. This scalogram reveals the change in foF2, h' F and hmF2 during the SSS as result of energy deposited

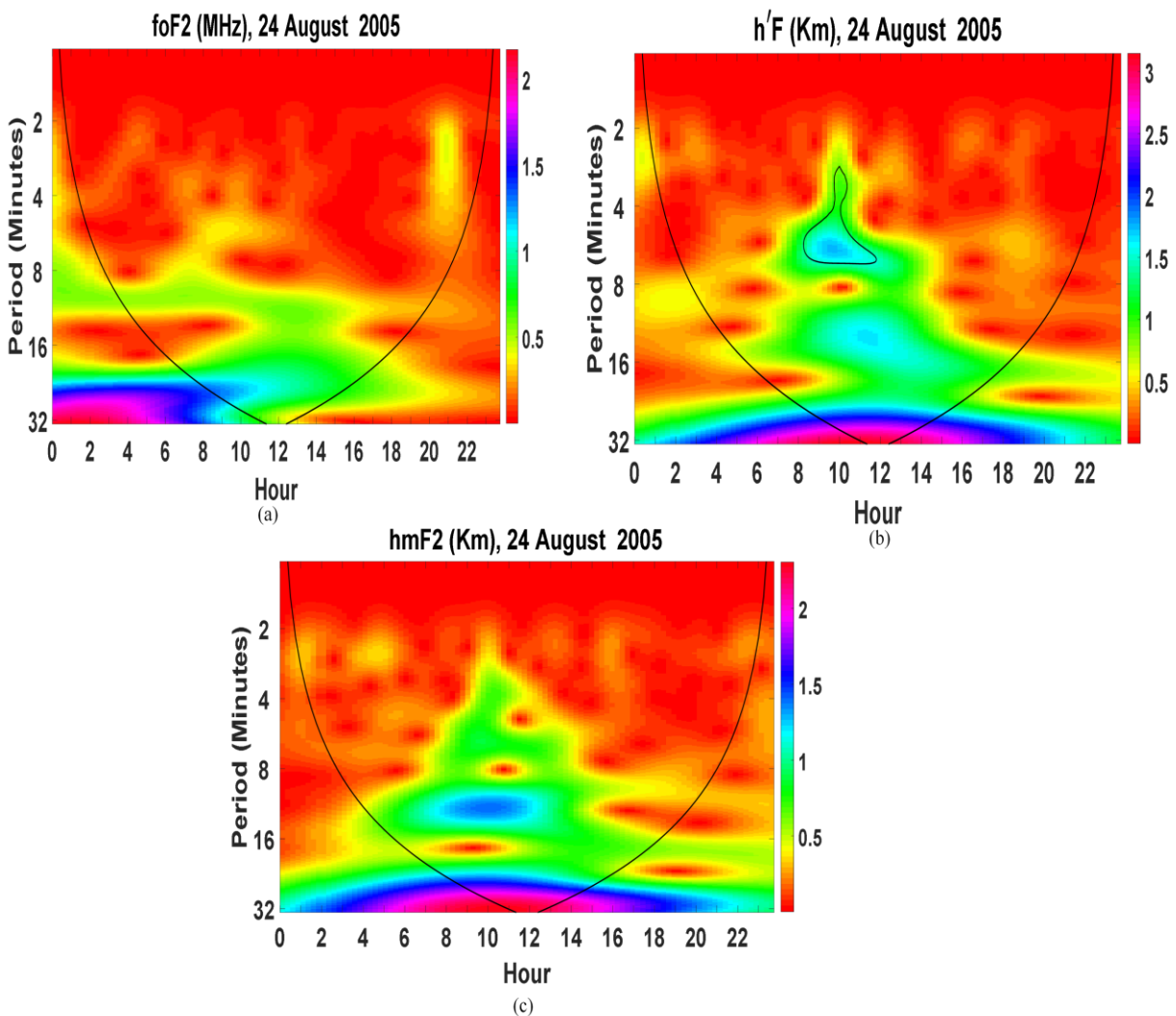


Fig. 6(a), (b) and (c) The scalogram of critical frequency (foF2 in MHz), virtual height(h' F in Km) and height of peak electron density (hmF2 in Km) on the SSS day of 24 August 2005.

in magnetosphere-ionosphere by coupling mechanism between geomagnetic field and southward component of IMF Bz. The injected energy and charge particle causes sudden increase in ionospheric current produces ionospheric storm along with variation in communication signal and power blackout in the Earth's surface. Figures 7a, b and c and the 8a, b and c are same as in figures 6a,b and c but it refers to the SSS events on 7 September 2017 and 8 September 2017. In figures 7a, b and c the power area of highest intensity is observed ~ 23:45 UT during SSS events with periods 27.9 to 64 minutes. The background intensity increased from 0.5 to 2 (nT)² for foF2, h' F and hmF2 respectively. Similarly, the power

area of highest intensity is observed ~13:00 UT during SSS with periods 27.9 to 64 minutes. The background intensity for foF2 increased from 1 to 3 (nT)²; for h' F increased from 1 to 4 (nT)² and for hmF2 increases from 0.5 to 2 (nT)² respectively. This quiescent and non-quiescent periods identified in foF2, h' F and hmF2 during southwards turning of IMF Bz is indicator of energy and particle injected during coupling mechanism between IMF Bz and geomagnetic field. In 2019, Bozhidar [32] analyzed large amount of heterogeneous data of geomagnetic indices, ionospheric parameters and IMF Bz using continuous wavelet transform and found the persistence of short-term period in it.

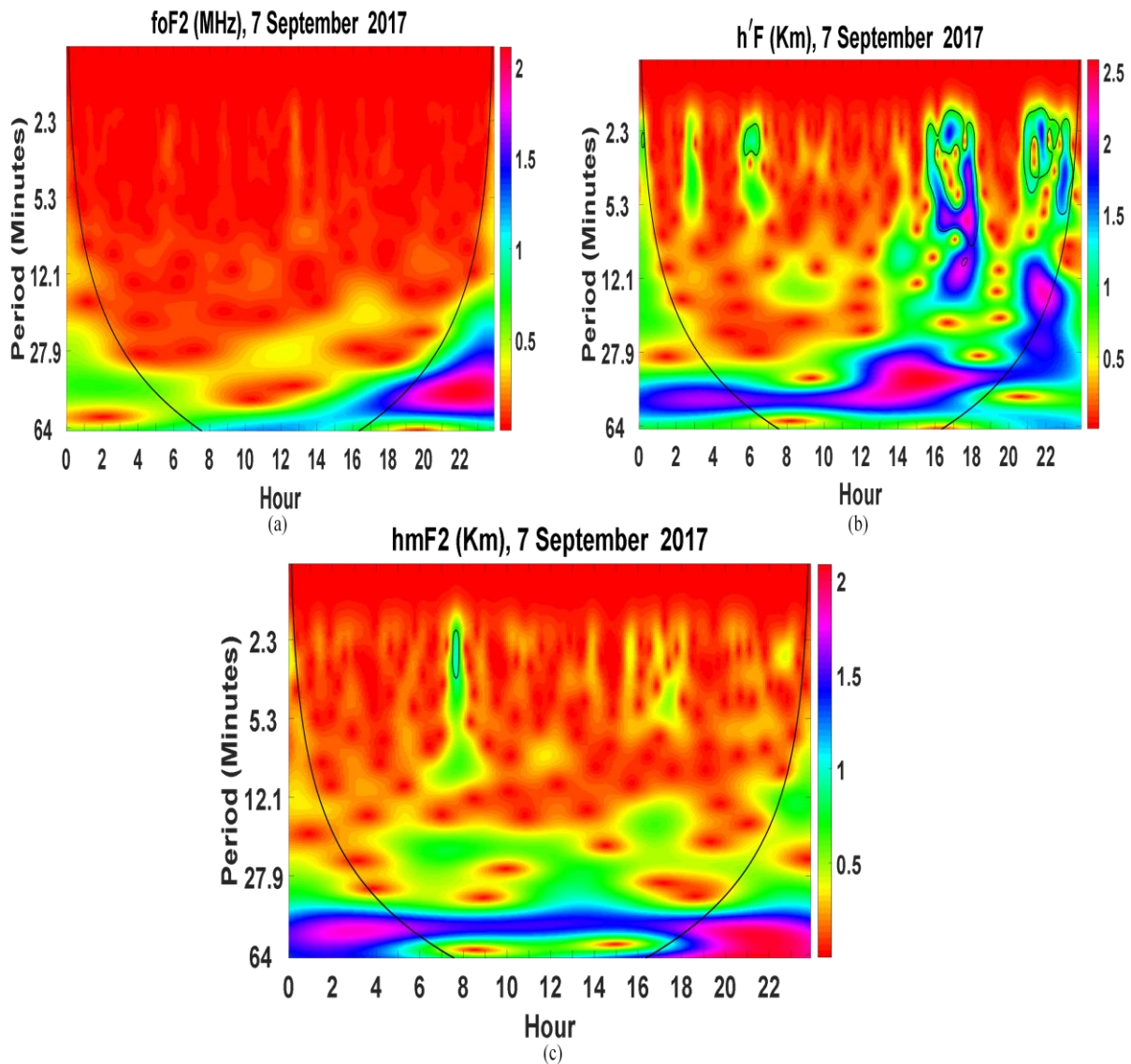


Fig. 7(a), (b) and (c) The scalogram of critical frequency (foF2 in MHz), virtual height (h' F in Km) and height of peak electron density (hmF2 in Km) on the SSS day of 7 September 2017.

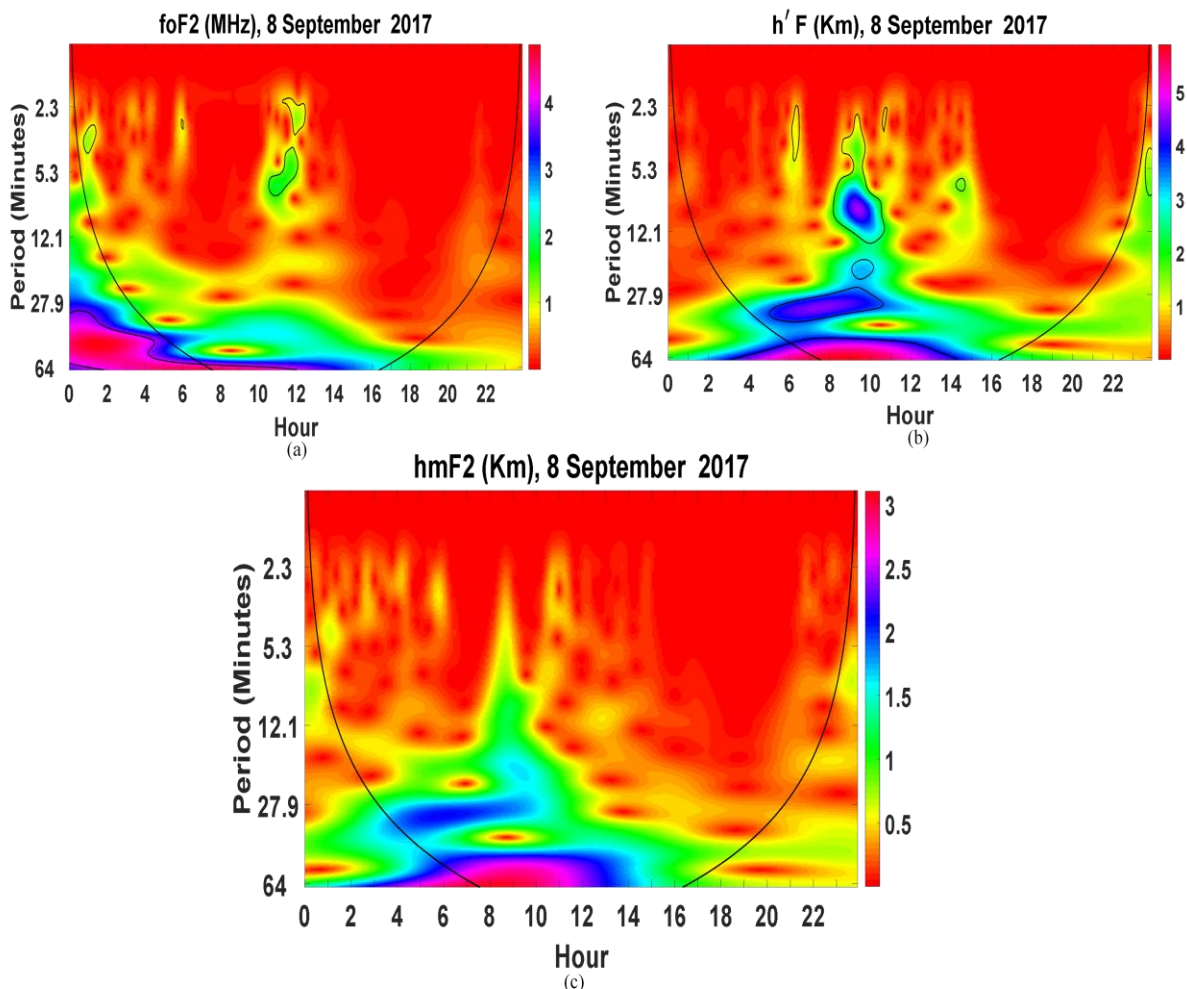


Fig. 8 (a), (b) and (c) The scalogram of critical frequency (foF2 in MHz), virtual height(h' F in Km) and height of peak electron density (hmF2 in Km) on the SSS day of 8 September 2017.

4. CONCLUSION

The mid latitude ionospheric responses on F2 layer critical frequency (foF2), virtual height (h' F) and peak height of electron density(hmF2) are analyzed using ionosonde data over Boulder, Colorado, USA (40°N, 1105.0° W) during super substorms of 24 August 2005, 7 September 2017 and 8 September 2017. The phenomena of decrease in foF2 during 24 August 2005 and 8 September 2017 SSSs caused by positive ionospheric storm and the increase in foF2 during SSS of 7 September 2017 caused by negative ionospheric storm was identified. The results of continuous wavelet transform (cwt) shows that the coupling between solar wind and magnetosphere occurs between ~16 to 32 minutes for SSS of 24 August 2005 and between 27.9 to 64 minutes during super substorm of 7 and 8 September 2017 for all the ionospheric parameters respectively. The highest fluctuation in h'F is noticed during SSS of 24 August 2005. This study provide concept of physical mechanism responsible for SSSs event which is still

lacking and are in progress in scientific community. The global picture of SSSs can be obtained only after taking into account the ionospheric data from global stations.

ACKNOWLEDGEMENTS

We acknowledge Omni data site (https://omniweb.gsfc.nasa.gov/form/omni_min.html) for providing data for solar wind, interplanetary parameters and geomagnetic indices. The special thanks are extended to the Global Ionospheric Radio Observatory (GIRO) website <https://ulcar.uml.edu/DIDBase/> for providing ionosonde data. The author would like to acknowledge Nepal Academy of Science and Technology (NAST), Nepal for proving PhD scholarship.

REFERENCES

- [1] Tsurutani, B. T.; Hajra, R.; Echer, E.; & Gjerloev, J. W. Extremely intense ($SML \leq 2500$ nT)

- substorms: Isolated events that are externally triggered?, *AnGeo. Comm.*, **33**: 519–524 (2015).
- [2] Lakshmi, D. R.; Veenabhari, B.; Dabas, R. S. & Reddy, B. M. Sudden post-midnight decrease in equatorial F-region electron densities associated with severe magnetic storms. *Annales Geophysicae, European, Geosciences Union*, **5** (3): 306–313 (1997). hal-00316203.
- [3] Pincheira, X. T.; Abdu, M. A.; Batista, I. S.; & Richards, P. G. An investigation of ionospheric responses, and disturbance thermospheric winds, during magnetic storms over South American sector, *J. Geophys. Res.*, **107** (A11): 1379 (2002).
- [4] de Abreu, A. J.; Fagundes, P. R.; Bolzan, M. J. A.; de Jesus, R.; Pillat, V. G.; Abalde, J. R.; Lima, W. L. C. The role of the traveling planetary wave ionospheric disturbances on the equatorial F region post-sunset height rise during the last extreme low solar activity and comparison with high solar activity. *J. Atmos. Sol-Terr. Phys.*, **113**: 47–57 (2014c).
- [5] de Abreu, A. J.; Fagundes, P. R.; Bolzan, M. J. A.; Gende, M.; Brunini, C.; de Jesus, R.; Pillat, V. G.; Abalde, J. R.; Lima, W. L. C. Traveling planetary wave ionospheric disturbances and their role in the generation of equatorial spread-F and GPS phase fluctuations during the last extreme low solar activity and comparison with high solar activity. *J. Atmos. Sol-Terr. Phys.*, **117**: 7–19 (2014a).
- [6] de Abreu, A. J.; Fagundes, P. R.; Gende, M.; Bolaji, O. S.; de Jesus, R.; Brunini, C. Investigation of ionospheric response to two moderate geomagnetic storms using GPS-TEC measurements in the South American and African sectors during the ascending phase of solar cycle 24. *Adv. Space Res.*, **53**: 1313–1328 (2014b).
- [7] Rungraengwajjake, S.; Supnithi, P.; Tsugawa, T.; Maruyama, T.; Nagatsuma, T. The variation of equatorial spread-F occurrences observed by ionosondes at Thailand longitude sector. *Adv. Space Res.*, **52**: 1809–1819 (2013).
- [8] Smith, J. M.; Rodrigues, F. S.; de Palua, E. R. Radar and satellite investigations of equatorial evening vertical drifts and spread F. *Ann. Geophys.*, **33**: 1403–1412 (2015).
- [9] Liu, G. Q. & Shen, H. A severe negative response of the ionosphere to the intense geomagnetic storm on March 17, 2015 observed at mid- and low-latitude stations in the China zone. *Adv. Space Res.* **59**: 2301–2312 (2017).
- [10] Manju, G.; Devasia, C. V.; Sridharan, R. On the seasonal variations of the threshold height for the occurrence of equatorial spread F during solar minimum and maximum years. *Ann. Geophys.*, **25**: 855–861 (2007).
- [11] Narayanan, V. L.; Gurubaran, S.; Berlin Shiny, M. B.; Emperumal, K. & Patil, P. T. Some new insights of the characteristics of equatorial plasma bubbles obtained from Indian region. *J. Atmos. Sol-Terr. Phys.*, **156**: 80–86 (2017).
- [12] Narayanan, V. L.; Sau, S.; Gurubaran, S.; Shiokawa, K.; Balan, N.; Emperumal, K.; Sripathi, S. A statistical study of satellite traces and evolution of equatorial spread F, *Earth Planets Space*, **66**: 160 (2014).
- [13] Hajra, R.; Tsurutani B. T.; Echer, E.; Gonzalez, W. D.; and Gjerloev, J. W. Supersubstorm (SML < 2500 nT) magnetic storm and solar cycle dependences, *J. Geophys. Res. Space Physics*, **121**: 7805–7816 (2016).
- [14] Adhikari, B.; Mishra, R. K.; Pandit, D.; Bhattarai, B.; and Chapagain, N. P. Ionospheric Effect of Non-Storm Hildca (High Intensity Long Duration Continuous Auroral Activity), *Journal of Institute of Science and Technology*, **22**: 2467-9240 (e) (2017c) ISSN: 2469-9062 (print).
- [15] Adhikari, B. P.; Baruwal, P. and Chapagain, N. P. Analysis of supersubstorm events with reference to polar cap potential and polar cap index, *Earth Space Sci.*, **4**: 2–15 (2017a).
- [16] Adhikari, B. S.; Dahal, S. and Chapagain, N. P. Study of field aligned current (FAC), interplanetary electric field component (Ey), interplanetary magnetic field component (Bz), and northward (x) and eastward (y) components of geomagnetic field during supersubstorm., *Earth and Space Science*, **4**: 257–274 (2017b). doi:10.1002/2017EA000258.
- [17] Despirak, I.; Kleimenova, N.; Gromova, L.; Gromov, S.; and Malysheva, L. Supersubstorms during strong magnetic storm on 7 September 2017, *E3S Web of Conferences*, **127**: 01010 (2019). doi.org/10.1051/e3sconf/2019127010.
- [18] Despirak, I. V.; Lubchich, A. A.; Kleimenova, N. G. Large-scale structure of solar wind and appearance of super substorms, *Physics of Auroral Phenomena, Proc. XLI Annual Seminar, Apatity*, 11-13 (2018). *Polar Geophysical Institute*.
- [19] Tsurutani, B. T.; Lakhin, G. S.; and Hajra, R. The physics of space weather/solar-terrestrial physics (STP): what we know now and what the current and future challenges are. *Nonlin. Processes Geophys.*, **27**: 75–119 (2020).
- [20] Daubechies, I. Ten lectures on wavelets [S.I.]: Society for Industrial and Applied Mathematics, PA, USA. (1992).
- [21] Meyer, Y. Ondelettes Et Operateurs, Hermann, Paris (1990).
- [22] Poudel, P.; Simkhada, S.; Adhikari, B.; Sharma, D.; & Nakarmi, J. J. Variation of solar wind parameters along with the understanding of

- energy dynamics within the magnetospheric system during geomagnetic disturbances. *Earth and Space Science*, **6**: 276–293 (2019).
- [23] Li, H.; Wang, J. S.; Chen, Z.; Xie, L.; Li, F. and Zheng, T. The contribution of geomagnetic activity to ionospheric foF2 trends at different phases of the solar cycle by SWM, *Atmosphere*, **11**: 616 (2020).
- [24] Belehaki, A. and Tsagouri, I. Investigation of the relative bottomside/topside contribution to the total electron content estimates, *Annals of geophysics*, (2002). DOI: 10.4401/ag-3498.
- [25] Pross, G. W. Ionospheric F-region storms, in *Handbook of Atmospheric Electrodynamics*, 195-248 (1995). II, CRC Press.
- [26] Rishbeth, H. How the thermospheric circulation affects the ionospheric F2-layer, *J. Atmos. Solar-Terr. Phys.* **60**: 1385-1402 (1998).
- [27] Pross, G. W.; Roemer, M. and Slowey, J. W. Dissipation of solar wind energy in the earth's upper atmosphere: The geomagnetic activity effect, CIRA 1986, *Adv. Space Res.* **8** (5): 215-261 (1998).
- [28] Mikhailov, A. V.; Yu, L.; Terekhin, M. G.; Skoblin, and Mikhailov, V. V. On the physical mechanism of the ionospheric storms in the F2-layer, *Adv. Space Res.*, **12** (10): 269-272 (1992).
- [29] Cander, L. R. and Mihajlovic, S. J. Forecasting ionospheric structure during the great geomagnetic storms, *J. Geophys. Res.*, **103**: 391-398 (1998).
- [30] Cander, L. R. On the global and regional behaviour of the mid-latitude ionosphere, *J. Atmos. Terr. Phys.* **55**: 1543-1551 (1993).
- [31] Pross, G. W. On explaining the local time variation of ionospheric storm effects, *Ann. Geophys.*, **11**: 1-9 (1993).
- [32] Bozhidar, S.; Ognyan, K.; Georgi, S. Wavelet Analysis of Big Data in the Global Investigation of Magnetic Field Variations in Solar-Terrestrial Physics, arXiv:1905.12923v1 [physics.space-ph] (2019).